Letters

A Dual-Output Rectifier-Based Self-Powered Interface Circuit for Triboelectric Nanogenerators

Yirui Su, *Graduate Student Member, IEEE*, Masao Yanagisawa, *Member, IEEE*, and Youhua Shi, *Member, IEEE*

***Abstract*—Triboelectric nanogenerators (TENGs) offer a cost-effective solution for harvesting energy in Internet of Things (IoT) devices. However, their practical application is limited due to extremely high output voltage and low intrinsic capacitance, alongside the nonself-powered nature of current interface circuits and low transfer efficiency resulting from output voltage asymmetry. Addressing these issues, this letter introduces a dual-output rectifier-based interface circuit, innovatively designed to rectify TENG output into two distinct voltage magnitudes, optimizing for energy harvesting and switching generation. The experimental results validate our approach, showing gains of 2.75 and 2.34 times in terms of maximum output power over a full-wave rectifier (FWR)-based design at 2 and 3 Hz, respectively. Furthermore, under identical frequency and load conditions (1 MΩ at 2 and 3 Hz), the output gains reached 152 and 160 times that of the FWR. Our approach brings about a significant advancement in TENG integration for low-frequency and low-load IoT devices. This letter is accompanied by two videos demonstrating the charge response of 1 MΩ load at 2 and 3 Hz, respectively.**

***Index Terms*—Energy harvesting (EH), interface circuit, self-powered, triboelectric nanogenerators (TENGs).**

I. Introduction

With the remarkable growth of the Internet of Things (IoT), various wearable electronics have seamlessly integrated into our daily life, creating a new dimension of interaction between humans and devices. To remove the battery reliance of these IoT devices, energy harvesting (EH) technologies, capable of collecting thermal, solar, electromagnetic, and kinetic energy from the ambient environment, have emerged as a promising solution. Among them, triboelectric nanogenerators (TENGs) introduced in [1] have gained wide recognition due to their cost-effectiveness, environmental friendliness, and impressive output for converting low-frequency mechanical energy into electricity.

Manuscript received 10 January 2024; revised 19 February 2024; accepted 5 March 2024. Date of publication 18 March 2024; date of current version 19 April 2024. This work was supported in part by Waseda University Grant for Special Research Projects under Grant 2023C-101. *(Corresponding author: Youhua Shi.)*

The authors are with the Faculty of Science and Engineering, Waseda University, Tokyo 169-8555, Japan (e-mail: yirui.su@islab.cs.waseda.ac.jp; yanagi@islab.cs.waseda.ac.jp; youhua.shi@islab.cs.waseda.ac.jp).

Color versions of one or more figures in this article are available at https://doi.org/10.1109/TPEL.2024.3376536.

Digital Object Identifier 10.1109/TPEL.2024.3376536

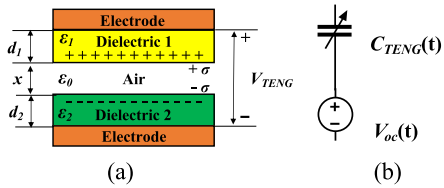

Fig. 1. (a) CS-TENG and (b) equivalent circuit of TENG.

TENGs operate based on contact electrification and electrostatic induction principles. As illustrated in Fig. 1(a), the process involves the generation of electrostatic charges on the surface of specific materials through contact and separation. These charges, driven by the resultant potential difference, flow between the electrodes. Thus, a TENG can be modeled as a series connection of a voltage source and a variable capacitor, as depicted in Fig. 1(b). Four fundamental TENG modes have been discussed in [2], of which the vertical contact-separation mode (CS-TENG) is the simplest and most commonly utilized. While efforts to enhance TENG power density and reliability have predominantly focused on material and structural optimization, TENG's inherent capacitance-based nature limits effective energy transfer to the load. Consequently, similar to other EH technologies, TENGs generally require an interface circuit to enhance energy transfer efficiency and achieve impedance matching with the connected load.

In the literature, numerous interface circuit designs have been proposed to enhance TENG output. Bennet's doubler [3] is an unstable charge pump that feeds charges from the load back to TENGs, increasing the output energy of TENGs exponentially but at the cost of the requirement of many external motion cycles. Synchronized switch harvesting on inductor (SSHI) [4], [5], introduces an inductor in series or parallel with a switch to provide an energy-returning path of TENGs to improve the corresponding output, but it will decay without an optimal load. Synchronous charge extraction (SCE) [6], [7], and prebiased synchronous charge extraction (pSCE) [7] can boost the output energy even under impedance mismatch between TENGs and the following load, but the self-powered manner of the interface circuit was not addressed. The fractal switched-capacitor converter (FSCC) presented in [8] and [9] is composed of multiple switched-capacitor pairs and utilizes a mechanical switch to

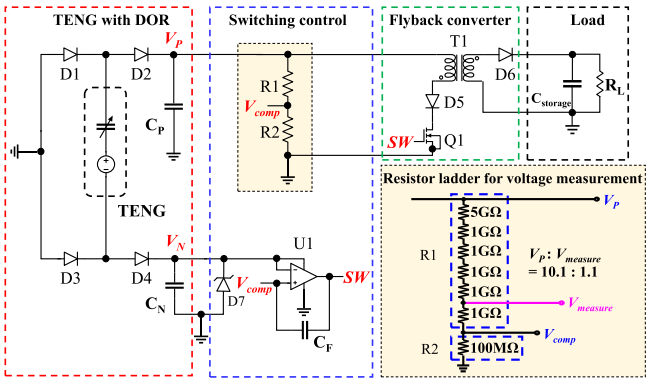

Fig. 2. Proposed DOR-based interface circuit. To measure V_P, we employed a voltage divider for indirect voltage measurement, where, instead of using a single 10 GΩ resistor as R1, a series combination of a 5 GΩ resistor and five 1 GΩ resistors was utilized. Thus, the voltage (V_{measure}) is measured with an oscilloscope, and then V_P is calculated by multiplying the observed voltage by a factor of 10.1/1.1.

automate the step-down conversion of high-voltage energy from TENGs, thereby enhancing output without the need for inductors. However, FSCC's efficiency may decrease if the actual voltage conversion ratio differs from the one predetermined by the fixed number of switched-capacitor pairs. Moreover, designs based on integrated circuits, such as the high-voltage dual-input buck converter [10], Multishot SCE with a buck–boost regulator [11], and SSHI featuring both a buck and a switched-capacitor dc–dc converter [12], face technological limitations, including the fact that the voltage levels they can handle are significantly lower than the open-circuit voltage of TENGs. This limitation restricts the amount of energy that can be effectively harvested from TENGs through these methods. In [13], a full-wave rectifier (FWR)-based interface circuit employing a silicon-controlled rectifier (SCR) combined with a Zener diode as a passive switch is utilized to harness TENG output energy. However, the imprecise control of the switch, comprising the SCR and Zener diode, only charges the load capacitance to the trigger voltage before discharging it, resulting in suboptimal energy transfer efficiency. Furthermore, the FWR-based ac–dc converter inherently limits TENG output energy due to the asymmetric voltage [14] caused by the converter.

As shown in Fig. 2, this letter proposes a novel and effective self-powered dual-output rectifier (DOR)-based interface circuit for CS-TENGs. In the proposed design, the TENG output is deliberately rectified to two distinct voltage magnitudes, optimizing for EH and switching generation. To minimize energy loss, we generate a step-down switching control signal by harnessing the energy of a TENG moving from separation to contact during the negative half cycle. Concurrently, the output of a TENG moving from contact to separation during the positive half cycle is stored in a temporary capacitor at the high voltage level, stepped down and transferred to the load via a flyback converter subsequently when the voltage level triggers the control module. This is done with the generated switching control signal to maximize energy transfer efficiency. As a result, both the low energy transfer efficiency issue caused by asymmetry and the need for an external power source for switching signal generation are addressed, paving the way for wider applications of TENGs.

II. Output Analysis of CS-TENG With DOR

To better understand the voltage and charge transfer mechanisms in a CS-TENG, we first analyze the output of a TENG with DOR alone (depicted as the red block in Fig. 2), which consists of four diodes (D1–D4) and two capacitors (C_P and C_N).

Following the analysis on "cycles for maximized energy output" in [15], the output energy per cycle of a CS-TENG with DOR can be expressed as

$$\begin{aligned} E_{\text{DOR}} &= V_P\,\Delta Q_P + V_N\,\Delta Q_N \\ &= (V_P + V_N)\,[C_{\min}V_{oc} - C_{\min}V_P - C_{\max}V_N] \end{aligned} \tag{1}$$

where ΔQ_P and ΔQ_N denote the transferred charges during the positive and negative half cycle, respectively. $C_{\max}$ and $C_{\min}$ are the maximum and minimum value of TENG's intrinsic capacitance. V_{oc} is the TENG's open circuit voltage, and V_P and V_N indicate the voltages across the two temporal capacitors C_P and C_N, respectively. For simplification, it is assumed that the voltages V_P and V_N remain constant in the steady-state mode.

From (1), E_{DOR}, which is the combined output from both the positive and negative half cycle, depends on the voltages of the temporal capacitors and the charges transferred. Furthermore, in the steady-state condition, the total amount of charge transferred during positive and negative half cycle should be equal, i.e., $\Delta Q_P{=}\Delta Q_N$. It is worth noting that the conventional rectifiers, such as FWR and half-wave rectifiers (HWR) can be viewed as specific cases of the DOR-based design. In the case of FWR, $V_P{=}V_N$, and for HWR, $V_N{=}\ 0$.

Let β denote the ratio of $C_{\max}$ to $C_{\min}$, following (1), thus the output energy per cycle of a CS-TENG with FWR and HWR can be expressed as

$$E_{\text{FWR}} = 2V_P\ [C_{\min}V_{\text{oc}} - (\beta+1)\,C_{\min}V_P] \tag{2}$$

and

$$E_{\text{HWR}} = V_P\ [C_{\min}V_{\text{oc}} - C_{\min}V_P] \tag{3}$$

respectively.

For energy to be harvested, the transferred charges in (1) must be positive, which implies that

$$V_{\text{oc}} > V_P + \beta V_N. \tag{4}$$

For DOR, (4) suggests that the upper limits for V_P and V_N will be V_{oc} (when $V_N{=}\ 0$) and V_{oc}/β (when $V_P{=}\ 0$), respectively, also demonstrating that V_P can reach higher voltage than V_N. As to FWR and HWR, the upper limits is $V_{\text{oc}}/(\beta{+}1)$ and V_{oc}, respectively.

To further study E_{DOR} from positive and negative half cycle, an LTSpice simulation is conducted on a CS-TENG with the parameters given in Table I, and Fig. 3 shows results of them with varying V_N. It can be observed that the output from positive half cycle is predominant because V_P can reach much higher levels than V_N as implication of (4). E_{HWR} and the maximum output under FWR are also noted in Fig. 3(a), demonstrating that the output potential of both DOR and HWR can be much

TABLE I
MEASURED ELECTRICAL PROPERTIES OF TENG

Parameters	Value
Maximum open circuit voltage	V_{oc}= 2500 V
Maximum TENG capacitance	C_{max}= 1150 pf
Minimum TENG capacitance	C_{min}= 105 pf
TENG intrinsic capacitance ratio	$\beta \approx 11$

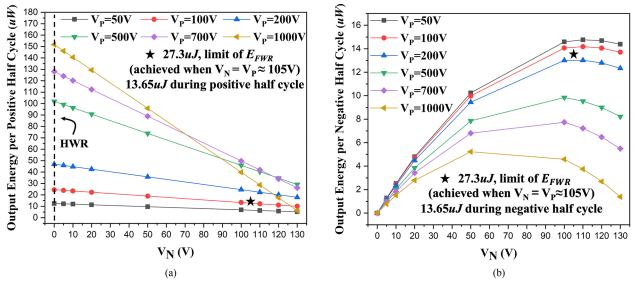

Fig. 3. (a) Output energy per positive half cycle varying with V_N. (b) Output energy per negative half cycle varying with V_N.

greater than that of under FWR as long as $\beta > 1$ due to the nature of the asymmetric voltage [14] caused by the FWR-based converter. Considering that DOR can rectify TENG's output to two orders of magnitude of different voltages, it is feasible to keep V_P as much as high and maintain V_N at a specified low level (e.g., 5 V). This enables efficient energy rectification from the positive half-cycle, while keeping that from the negative half-cycle minimal yet adequate for generating switching signals in a self-powered manner.

III. PROPOSED DOR-BASED SELF-POWERED DESIGN

The proposed interface circuit, shown in Fig. 2, primarily consists of a DOR, a flyback converter, and a self-powered switching control module. The energy harvested during the positive half cycle is stored in C_P until the MOSFET switch (Q1) closes, while the energy collected during the negative half cycle is employed as the power supply and reference voltage for the switching control module. With respect to the two outputs in DOR, V_P is divided by a voltage divider, formed by resistors R_1 and R_2, to generate V_{comp} for comparison. In contrast, V_N, clamped by the Zener diode (Typ. 5.6 V), powers the nano power comparator, U1. Subsequently, the voltage V_{comp} and V_N are compared through U1, generating the switching control signal for the MOSFET, Q1.

It is worth mentioning that to prevent the generation of an overlapping switch signal due to the decrease of V_N when the TENG moves from separation to contact, presenting a risk of inadvertently triggering the comparator and subsequently activating the MOSFET switch, a comparator with built-in hysteresis is used. Furthermore, to mitigate the risk of increased switching losses due to multiple energy transfers, a feedback capacitor C_F is added between the positive input and output of the comparator. This enhancement boosts the hysteresis effect, ensuring that the divided V_{comp} consistently stays below the minimum V_N after

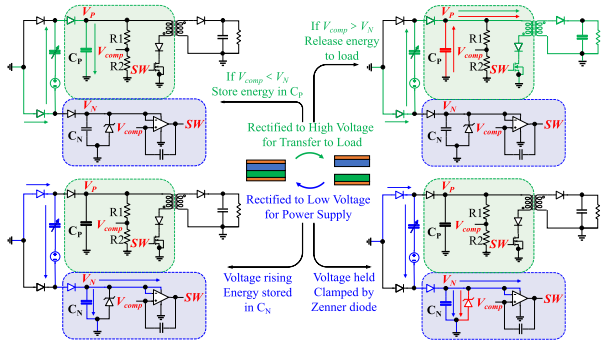

Fig. 4. Operation principle of the proposed interface circuit.

V_P releases energy. Consequently, this design adjustment effectively prevents the comparator from being erroneously triggered by the decreased V_N, thus enabling the system to discharge approximately once per cycle.

The operation principle of the proposed circuit is shown in Fig. 4. When $V_{\text{comp}} < V_N$, the MOSFET remains OFF, resulting in the proportional rise of V_{comp} and V_P. Once V_{comp} surpasses V_N, the comparator activates the MOSFET. The threshold voltage enabled to transfer the energy of V_P is

$$V_{P,\text{TH}} = V_N \cdot \left(1 + \frac{R_1}{R_2}\right). \tag{5}$$

Consequently, the output only from the positive half cycle is transferred to the flyback transformer and the following load subsequently. The output energy can be theoretically calculated as

$$\begin{aligned} E_{\text{Proposed}} &= V_{P,\text{TH}} \cdot \Delta Q_P \\ &= V_{P,\text{TH}} \cdot [C_{\text{min}} V_{\text{oc}} - C_{\text{min}} V_{P,\text{TH}} - C_{\text{max}} V_N]. \end{aligned} \tag{6}$$

Similar to the above analysis, the energy dissipated by the Zener diode and the comparator during the negative half cycle can theoretically written as

$$\begin{aligned} E_{\text{Dissipated}} &= V_N \cdot \Delta Q_N \\ &= V_N \cdot [C_{\text{min}} V_{\text{oc}} - C_{\text{min}} V_{P,\text{TH}} - C_{\text{max}} V_N]. \end{aligned} \tag{7}$$

Considering that R_1 and R_2 used in the circuit are 10 GΩ and 100 MΩ, respectively, the energy dissipated ($E_{\text{Dissipated}}$) by the Zener diode and the comparator constitutes approximately 1% of the total energy (E_{Proposed}). However, it is important to note that the actual impact on the overall output power slightly exceeds this percentage due to the intrinsic limitations in energy transfer efficiency within our proposed system.

It is worth noting that as the higher $V_{P,\text{TH}}$, E_{Proposed} will theoretically increase, as illustrated in Fig. 3. On the other hand, for off-the-shelf TENGs with micro/nano-power output energy, the control module with the nano-power consumption is selected inevitably. Accordingly, considering the limited power driven by the control module without using any external drivers directly, a small signal MOSFET with a breakdown voltage rated at 600 V is selected in our experimentation.

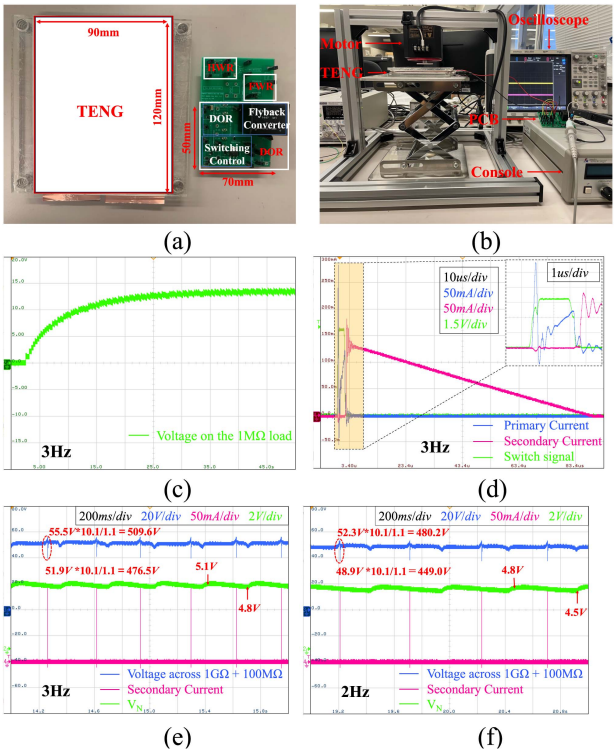

Fig. 5. Experimental setup and the corresponding waveforms. (a) Photograph of the self-manufactured CS-TENG and PCB. (b) Experimental setup. (c) Output voltage on a 1 MΩ load at 3 Hz. (d) Output responses of primary current, secondary current, and switch signal with enlarged view. (e) Voltage across 1 GΩ + 100 MΩ resistors and V_N with 3 Hz excitations. (f) Voltage across 1 GΩ + 100 MΩ resistors and V_N at 2 Hz.

IV. Experimental Results and Discussions

A. Device and Circuit Fabrication

Our self-manufactured CS-TENG employs a spring-assisted separation structure and consists of two copper sheets and a polytetrafluoroethylene (PTFE) sheet. The TENG's effective contact area measures 120 mm × 90 mm. The PTFE sheet in the TENG is 0.1 mm thick, with a maximum displacement of 1.2 mm in our experiments. Fig. 5(a) illustrates the self-manufactured TENG and PCB, while Table I presents the measured electrical properties of the TENG. For comparative evaluation, FWR, HWR, and the proposed DOR-based designs have been implemented on the same PCB. The experimental setup is depicted in Fig. 5(b), where the top plate of the TENG is driven in a reciprocating motion by a WaveMaker, with the frequency controlled by the vibration console.

B. Evaluation Results

Given that voltages like V_{oc} and V_P can escalate to kilovolts and are significantly affected by the input impedance of the measuring instrument, using a standard probe for measuring the voltage and output waveform at the node directly connected to the TENG body is impractical due to the requirement for ultra-high impedance (over ten of GΩ at several HZ). Therefore, like the method introduced in [16], we employed a voltage follower (OPA445) in conjunction with a voltage divider for indirect voltage measurement. To measure V_P, a series combination of

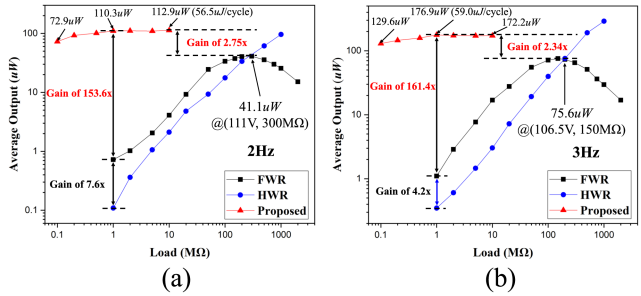

Fig. 6. Output power with varying loads at (a) 2 Hz and (b) 3 Hz.

a 5 GΩ resistor and five 1 GΩ resistors was utilized instead of a single 10 GΩ resistor as R_1, in order to accommodate the operating voltage range. The voltage across these combined resistors (1 GΩ + 100 MΩ) was monitored using the OPA445 as the voltage follower, and then V_P was derived by multiplying the observed voltage by a factor of 10.1/1.1.

For exhibiting the enhanced output energy of TENG with our proposed circuit in sub-5 Hz practical applications, the results of TENG working under 2 and 3 Hz are acquired in the experiment. Fig. 5(c) shows the charge response of 1 MΩ load at 3 Hz, the load is charged about to 13.3 V, corresponding an output of 176.9 μW. Fig. 5(d) shows the primary current, secondary current, and switching signal, with an enlarged view of the primary current and switching signal. The switch-ON period is approximately 2.5 μs, during which V_P decreases, and the energy stored in C_{TENG} transfers to the primary coil, leading to a surge current in the primary coil, of which energy is transferred to the second coil subsequently with the switch off. It is worth noting that our circuit deliberately excludes the use of gate resistors or snubber/clamp circuits to dampen the ringing. This is because a suboptimal design of these elements would result in greater losses than not using them at all. For instance, a gate resistor could increase switching losses, and snubber/clamp circuits could absorb more energy than they are designed to transfer, thereby dissipating more energy than they are designed to transfer. Fig. 5(e) shows the corresponding waveform of V_N and the voltage across the combined 1 GΩ + 100 MΩ resistors for the TENG with 3 Hz excitations and 1 MΩ load resistor. V_N, used for power supply and reference voltage, exhibits ripples from 4.8 to 5.1 V at 3 Hz. The system transmits energy to the load once V_P reaches 509.6 V and continues to do so until the voltage reduces to around 476.5 V. Due to the use of nano-power elements, the proposed circuit can also operate with 2 Hz excitations. As shown in Fig. 5(f), with 2 Hz excitations, V_N ripples from 4.5 to 4.8 V which is smaller than that of at 3 Hz. This reduction is attributed to the decreased energy C_N obtained from the TENG during the negative half cycle, leading to a lower Zener voltage that is maintained. Consequently, the system transmits energy once V_P reaching 480.2 V and continues to do so until the voltage reduces to around 449.0 V.

Fig. 6 presents a comparison of the output power among FWR, HWR, and our proposed DOR-based circuits with varying load resistances at 2 and 3 Hz excitations, in which the load resistance ranges from 100 KΩ to 10 MΩ, targeting practical applications. At 2 Hz, the output power of the TENG with

TABLE II
COMPARISON WITH OTHER INTERFACE CIRCUITS

Reference	[3]	[4]	[7]	[7]	[11]	[12]	[13]	This work
Process	Discrete	Discrete	Discrete	Discrete	0.18 μm BCD	0.18 μm BCD	Discrete	Discrete
Rectifier	Bennet's doubler	S-SSHI	SCE	pSCE	Multishoot SCE	P-SSHI	FWR	DOR
Regulation	-	-	-	-	BUCK–BOOST	BUCK+SCC	BUCK	Flyback
Self-Powered	Yes	No	No	No	No	Yes	Yes	Yes
Frequency (Hz)	5	10	10	10	60	5	3.3	2
Measurement Load (V)	- (Capacitor load)	5.69 @ 10 MΩ	10 (Battery load)	10 (Battery load)	27.2	2	22.4 @ 2 MΩ	10.5 @ 1 MΩ
Harvested Power Gain over FWR	21×	2.43×	2.7×	4.9×	1.91× *	1.62×	0.843× *	2.75× *

* Power gain is measured based on the maximum output power of the FWR.

our proposed circuit was 72.9, 110.3, and 112.9 μW for load resistances of 100 KΩ, 1 MΩ, and 10 MΩ, respectively. This represented a maximum gain of 274.7% over the highest output of the FWR. At 3 Hz, the output power for load resistances of 100 KΩ, 1 MΩ, and 10 MΩ were 129.6, 176.9, and 172.2 μW, respectively, corresponding to gains of 171.4%, 234.0%, and 227.8% over the FWR's maximum output. Furthermore, under identical conditions (1 MΩ load at 2 and 3 Hz), the output gains with the proposed circuit reached up to 153.6 and 161.4 times those of the FWR-based design. For comparison, Table II summarizes recently reported interface circuits and their key performance metrics. These results clearly demonstrate that our proposed DOR-based self-powered interface circuit can produce satisfying output even with ultra-small loads.

V. CONCLUSION

A novel self-powered interface circuit utilizing a DOR is proposed for contact-separation TENGs. This circuit effectively rectifies the output into two distinct voltage magnitudes, specifically optimized for EH and self-powered switching generation. Experimental results indicate a substantial improvement in performance over traditional FWR and HWR-based designs, even under low-frequency and low-load conditions. Consequently, this approach holds the potential to significantly advance the integration of TENGs as a reliable and independent power source in a variety of IoT applications.

REFERENCES

[1] S. Wang, L. Lin, and Z. L. Wang, "Nanoscale triboelectric-effect-enabled energy conversion for sustainably powering portable electronics," *Nano Lett.*, vol. 12, no. 12, pp. 6339–6346, 2012.
[2] S. Niu and Z. L. Wang, "Theoretical systems of triboelectric nanogenerators," *Nano Energy*, vol. 14, pp. 161–192, 2015.
[3] A. Ghaffarinejad et al., "A conditioning circuit with exponential enhancement of output energy for triboelectric nanogenerator," *Nano Energy*, vol. 51, pp. 173–184, 2018.
[4] X. Li and Y. Sun, "An SSHI rectifier for triboelectric energy harvesting," *IEEE Trans. Power Electron.*, vol. 35, no. 4, pp. 3663–3678, Apr. 2020.
[5] M. Pathak and R. Kumar, "Synchronous inductor switched energy extraction circuits for triboelectric nanogenerator," *IEEE Access*, vol. 9, pp. 76938–76954, 2021.
[6] X. Cheng et al., "High efficiency power management and charge boosting strategy for a triboelectric nanogenerator," *Nano Energy*, vol. 38, pp. 438–446, 2017.
[7] M. Pathak and R. Kumar, "Self-propelled pre-biased synchronous charge extraction circuit for triboelectric nanogenerator," *IEEE J. Emerg. Sel. Topics Power Electron.*, vol. 11, no. 1, pp. 615–626, Feb. 2023.
[8] W. Tang et al., "A power-transformed-and-managed triboelectric nanogenerator and its applications in a self-powered wireless sensing node," *Nanotechnology*, vol. 25, no. 22, Jun. 2014, Art. no. 225402.
[9] W. Liu et al., "Switched-capacitor-convertors based on fractal design for output power management of triboelectric nanogenerator," *Nature Commun.*, vol. 11, no. 1, 2020, Art. no. 1883.
[10] I. Park, J. Maeng, D. Lim, M. Shim, J. Jeong, and C. Kim, "A 4.5-to-16μW integrated triboelectric energy-harvesting system based on high-voltage dual-input buck converter with MPPT and 70V maximum input voltage," in *Proc. IEEE Int. Solid-State Circuits Conf.*, 2018, pp. 146–148.
[11] M. Pathak, S. Xie, C. Huang, and R. Kumar, "High-voltage triboelectric energy harvesting using multi-shot energy extraction in 70-V BCD process," *IEEE Trans. Circuits Syst. II: Exp. Briefs*, vol. 69, no. 5, pp. 2513–2517, May 2022.
[12] I. Kara, M. Becermis, M. A.-A. Kamar, M. Aktan, H. Dogan, and S. Mutlu, "A 70-to-2 V triboelectric energy harvesting system utilizing parallel-SSHI rectifier and DC-DC converters," *IEEE Trans. Circuits Syst. I: Reg. Papers*, vol. 68, no. 1, pp. 210–223, Jan. 2021.
[13] W. Harmon et al., "Timing strategy for boosting energy extraction from triboelectric nanogenerators," *Nano Energy*, vol. 85, 2021, Art. no. 105956.
[14] Z. Wang et al., "Two voltages in contact-separation triboelectric nanogenerator: From asymmetry to symmetry for maximum output," *Nano Energy*, vol. 69, 2020, Art. no. 104452.
[15] Y. Zi et al., "Standards and figure-of-merits for quantifying the performance of triboelectric nanogenerators," *Nature Commun.*, vol. 6, 2015, Art. no. 8376.
[16] H. Zhang et al., "Employing a MEMS plasma switch for conditioning high-voltage kinetic energy harvesters," *Nature Commun.*, vol. 11, 2020, Art. no. 3221.